ANALYSIS OF PALSAR-2 IMAGES TO EXTRACT GEOLOGICAL EFFECTS CAUSED BY THE 2018 HOKKAIDO-EASTERN-IBURI EARTHQUAKE

Fumio Yamazaki[1] and Wen Liu[2]
1. Research Fellow, National Research Institute for Earth Science and Disaster Resilience, Tsukuba, Japan
2. Assistant Professor, Chiba University, Chiba, Japan
Email: fumio.yamazaki@bosai.go.jp, wen.liu@chiba-u.jp

ABSTRACT

An Mw 6.6 earthquake hit the eastern part of Iburi sub-prefecture, Hokkaido, Japan on September 6, 2018. The occurrences of extensive liquefaction were reported in Tomakomai, Sapporo, Kita-Hiroshima cities. In this study, multi-temporal PALSAR-2 images acquired before and after the event were employed to extract ground failures in urban areas. The coherence values were calculated for pre-event and co-event PALSAR-2 image pairs. Comparing with the result of field surveys, the ground failures caused by liquefaction were identified properly by the reduction of coherence.

Keywords: 2018 Hokkaido-Eastern-Iburi earthquake, liquefaction, field survey, PALSAR-2

INTRODUCTION

After a large-scale natural disaster strikes, gathering damage information is quite important for emergency response and recovery activities. But the access to the affected areas is often hindered by the disruption of road networks and telecommunication systems. Hence remote sensing technologies have been conveniently used to assess the extent and degree of various damages (Yamazaki and Matsuoka, 2007; Rathje and Adams, 2008; Dell'Acqua and Gamba; 2012). Various high-resolution optical and Synthetic Aperture Radar (SAR) satellites have been in operation in the recent years and they were employed to observe affected areas after major natural disasters such as the 2011 Tohoku-Oki, Japan, earthquake and tsunami (Liu et al., 2013), the 2015 Gorkha, Nepal, earthquake (Tsuchida et al., 2015), and the 2016 Kumamoto, Japan, earthquake (Liu and Yamazaki, 2017). The acquired satellite data provided the information on inaccessible affected areas.

SAR sensors can be used all day and under all weather conditions, and hence they are suitable for emergency data acquisition. Several frequency bands have been commonly used for satellite SAR systems, such as L-band (1 - 2 GHz: JERS-1, ALOS PALSAR, ALOS-2 PALSAR-2), C-band (4 - 8 GHz: ERS-1/2, ENVISAT, Radarsat-1/2, RISAT-1, Sentinel-1), and X-band (8 - 12 GHz: TerraSAR-X, COSMO-SkyMed). Among these frequency bands, the L-band is suitable to observe coherent changes such as ground deformation while the X-band is suitable to observe manmade objects and small-scale changes.

In this paper, multi-temporal PALSAR-2 images acquired before and after the 2016 Hokkaido-Eastern-Iburi, Japan, earthquake are introduced to extract ground failures caused by liquefaction in urban areas. The coherence values are calculated for pre-event and co-event PALSAR-2 pairs and the result is compared with that from field surveys.

THE 2018 HOKKAIDO-EASTERN-IBURI EARTHQUAKE AND PALSAR-2 DATA

An M_w 6.6 (M_J 6.7) earthquake hit the eastern part of Iburi sub-prefecture, Hokkaido, Japan on September 6, 2018 at 3:08 (JST). The epicenter was located in the mid-eastern part of Iburi sub-prefecture (the border of Atsuma and Mukawa Towns) with the depth 37 km (Japan Meteorological Agency (JMA), 2018). The earthquake was caused by a reverse fault system of high (74 degrees) dip

angle, running almost from the north to the south (358 degrees) as shown in Fig. 1 (Geospatial Information Authority of Japan (GSI), 2018). The figure also shows the distribution of the JMA Seismic Intensity, estimated by spatial interpolation (National Research Institute for Earth Science and Disaster Resilience (NIED), 2018). A large number of landslides were caused by this event due to strong shaking in the near source mountainous area. A total of 42 deaths were reported, mostly (36 people) involved by landslides in Atsuma Town. The total number of severely damaged residential buildings was 462, including 222 in Atsuma Town, 93 in Abira Town, 30 in Mukawa Town, 95 in Sapporo City, and 17 in Kita-Hiroshima City (Cabinet Office of Japan, 2019). The occurrence of extensive liquefaction was also reported in Sapporo and Kita-Hiroshima Cities, which was responsible for the building damage in the areas.

Figure 2 shows the study area and the color composite of the three-temporal PALSAR-2 images used in the study. The three temporal PALSAR-2 images were taken on 9 and 23 August, 2018 (pre-event) and on 6 September, 2018 (post-event), almost at the same time of the day (22:38 in local time). The L-band SAR images were acquired by StripMap mode with HH polarization from the ascending path with left look (slant range: 254 degrees from the north). The incident angle was 42.9 degrees and the spatial resolution was 1.43 m to the range direction and 1.77 m to the azimuth direction. The imagery data were provided by complex data of Level 1.1, preserving both the amplitude and phase information.

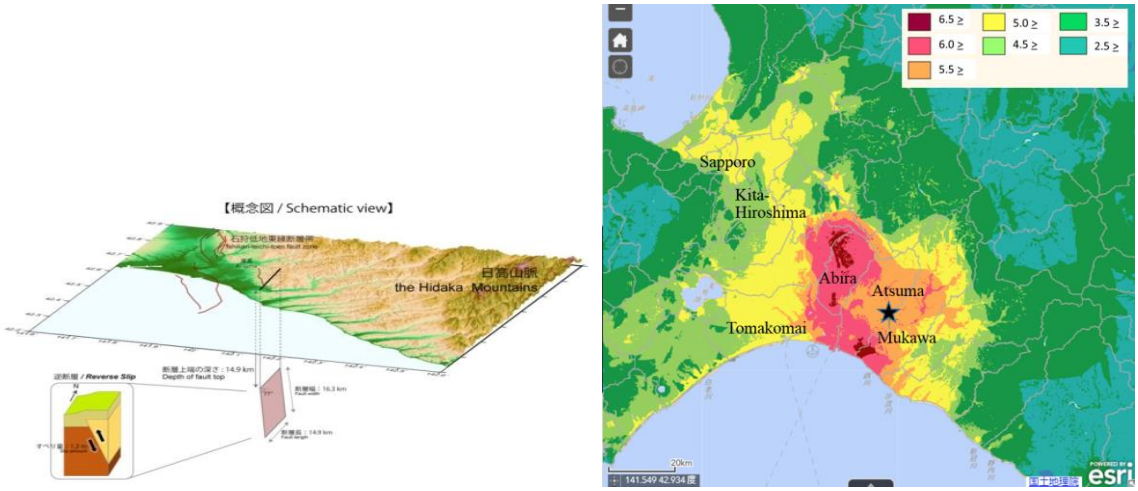

(a) (b)

Figure 1. (a) The source model of the 2018 Hokkaido-Eastern-Iburi earthquake by GSI (2018) and (b) the estimated JMA seismic intensity distribution by NIED (2018)

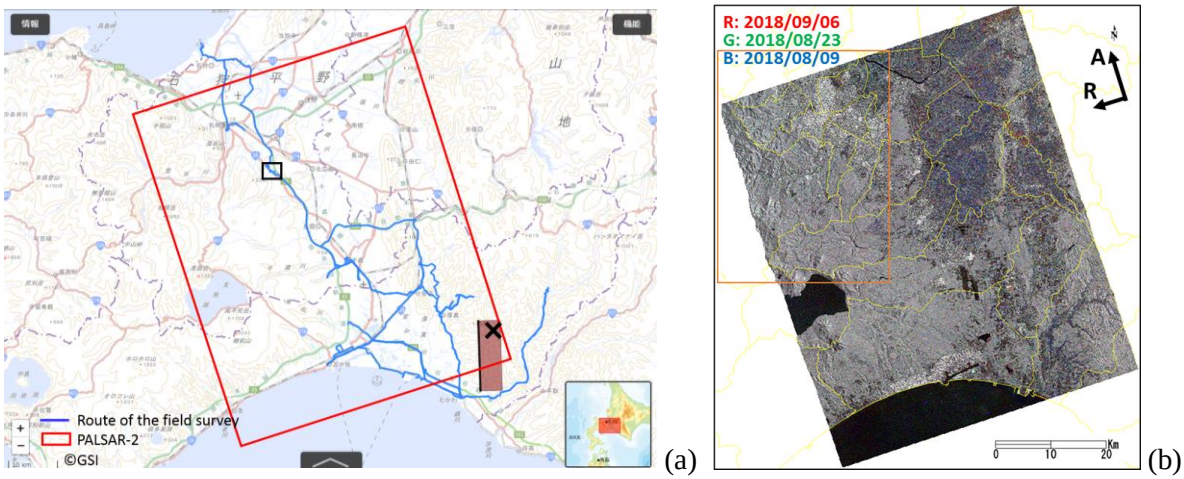

(a) (b)

Figure 2. (a) The study area and the location of PALSAR-2 images and (b) color composite of the three-temporal PALSAR-2 images

FIELD SURVEY

From 2nd to 4th October, 2018, about four weeks after the Eastern-Iburi earthquake, a team consisting of the current authors conducted field investigation to gather ground truth data. The route of the field survey was also plotted in **Fig. 2**(a) by blue line. We observed ground failure and liquefaction induced damages in Sapporo and Kita-Hiroshima on October 2. Many landslides were observed in Atuma and Abira Towns on October 3, and damages to roads, railways, and buildings were investigated in Mukawa Town and Tomakomai City on October 4.

Figure 3(a) shows an aerial photograph of a part of Sapporo and Kita-Hiroshima Cities, where building damages associated by liquefaction were observed. The aerial photo was taken by the Geospatial Information Authority of Japan (GSI) on September 13, 2018, one week after the earthquake. The photo was taken vertically and then orthorectified, and thus it was difficult to observe the inclination of buildings due to ground failures. Restoration works had been already carried out for damaged roads due to liquefaction. But gathered boiled sands and blue-colored polyethylene sheets covering damaged roofs show us the locations of heavily affected areas in Satozuka and Utsukushigahara, Kiyota Ward, Sapporo City. But the affected area in Ohmagari-Namiki, Kita-Hiroshima City was difficult to observe from the aerial photo because of many trees.

Figure 3(b) shows the field survey photographs taken at the three locations of ground failure. Photos 1 and 2 were taken at Satozuka-Ichijo, where extensive ground failures occurred. Satozuka area was developed as a residential area of wooden houses in 1970-80 by filling a valley of rice paddy fields (Nishimura and Watanabe, 2018). In the area, the ground surface was settled down 1-2 m unevenly. An extensive liquefaction was considered to occur in underground filled sand layers and liquefied soil flew downward along the slopping base layer. A wooden house without pile foundation was inclined but one with pile foundation was standing normally, as shown in Photo 2.

In Utsukushigaoka, the occurrence of liquefaction was reported by several researchers (Wakamatsu and Onoue, 2018; Nishimura and Watanabe, 2018) due to the 2018 event at the similar locations as those in the 2003 Tokachi-oki earthquake (M_w 8.0). We could still observe cracks (Photo 3) on the ground surface of a park, but damages to road pavement had already been repaired (Photo 4) at the time of our field survey. In Ohmagari-Namiki, concrete retaining walls were fell down to a small creek and the houses were displaced to the creek (Photos 5, 6). It was not clear whether the lateral and vertical displacements were caused by liquefaction or strong seismic motion.

(a) (b)

Figure 3. (a) Orthorectified aerial photograph of a part of Sapporo and Kita-Hiroshima Cities taken by GSI (2018) on September 13, 2018 and the route of our field survey on October 2, 2018 by blue line. (b) Photos take in our field survey at Satozuka (1, 2), Utsukushigaoka (3, 4), and Ohmagari-Namiki (5, 6).

EXTRACTION OF LIQUEFACTION AFFECTED AREAS FROM PLASAR-2 DATA

The three temporal PALSAR-2 images were processed by ENVI-SARscape software. Multi-look processing (2 looks each to the azimuth and range directions) was applied to the original images. A digital elevation model by GSI was used to compensate the image distortion caused by the terrain heights. Then they were projected to a World Geodetic System (WGS) 84 reference ellipsoid with a re-sampled square pixel size of 2.5 m. The amplitude information was converted to the backscattering coefficient (sigma naught: σ_0) in the dB unit, according to the calibration factor (Japan Aerospace Exploration Agency (JAXA), 2018).

In the color composites of the backscattering coefficient shown in Fig. 2(b), colored areas are observed in agricultural lands due to the seasonal difference between the three SAR images, but it is basically mono tone. Because of the spatial resolution of the SAR data, it was difficult to observe the surface changes due to liquefaction in Sapporo and Kita-Hiroshima Cities described before. Hence, the coherence (γ), which is the interferometric correlation between two SAR complex data, was calculated by the ratio between coherent and incoherent summations as Eq. 1.

$$\gamma = \frac{\sum C_1 C_2^*}{\sqrt{\sum |C_1|^2}\sqrt{\sum |C_2|^2}}, \tag{1}$$

where C is a complex number with phase (ϕ) and amplitude (A) and * denotes the complex conjugate. The estimated absolute value of γ, which ranges between 0 and 1, is the function of systemic spatial de-correlation (noise) and temporal de-correlation between the master and slave acquisitions.

The pre-event coherence (γ_{pre}) between the image on August 23, 2018 (master) and the one on August 9, 2018 (slave) was calculated from the complex SAR data. In the same manner, the co-event coherence (γ_{co}) was obtained from the master image on August 23, 2018 and the slave image on September 6, 2018. Then the color composite of the pre- and co-event coherence values and their histograms are shown in Fig. 4. The change between the two coherence values is clearly seen in mountainous and agricultural lands due to change by the earthquake and vegetation. Since the objective of this research is the extraction of ground failures in urban areas, urban land cover was extracted first by its high coherence value. From the histogram of the pre-event coherence, the pixels with $\gamma_{pre} \geq 0.68$ were considered as in urban areas. Then the difference of the two coherence values was calculated by

$$\Delta\gamma = \gamma_{co} - \gamma_{pre} \tag{2}$$

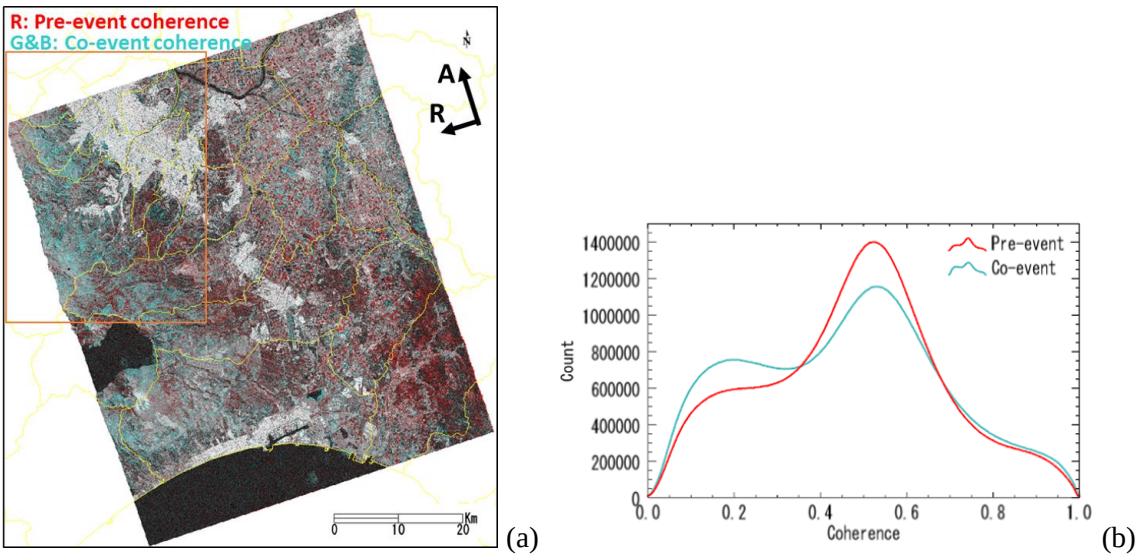

Figure 4. (a) Color composite of the pre-event (August 9 and 23, 2018) and co-event (August 23 and September 6, 2018) coherence values and (b) the histograms of the coherence values

The coherence difference, which is often used as the index to extract liquefaction affected areas (Ishitsuka et al., 2013), was shown for the extracted urban area in Fig. 5. In this figure (a), the areas with reduced coherence (blue color pixels) were also seen in two more locations outside of the surveyed area (b). By examining aerial photos, these locations were found to be agricultural lands where harvesting might be conducted before September 6, 2018. In the area including the three surveyed areas (b), the reduction of coherence was clearly observed at two more locations in Kiyota district of Kiyota Ward, which means some change occurred in the co-event period. Although we did dot visit these places, damages caused by liquefaction were reported (Nishimura and Watanabe, 2018).

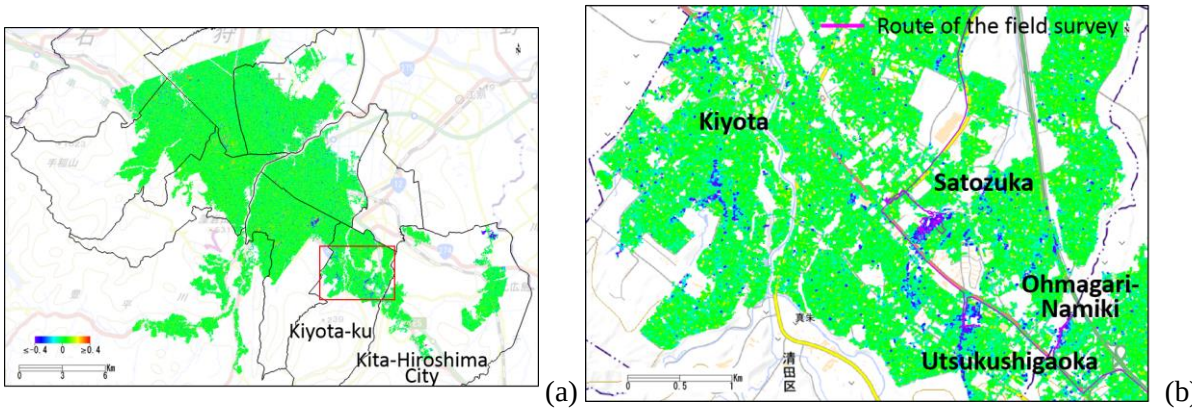

(a) (b)

Figure 5. (a) The coherence difference for the study area in orange-color square in Fig. 4(b) in rainbow color and (b) the enlargement of the red square in figure (a)

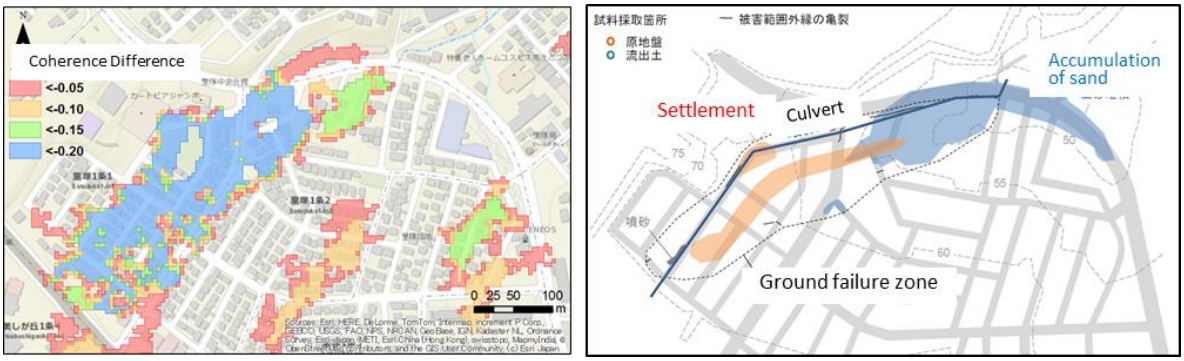

(a) Satozuka

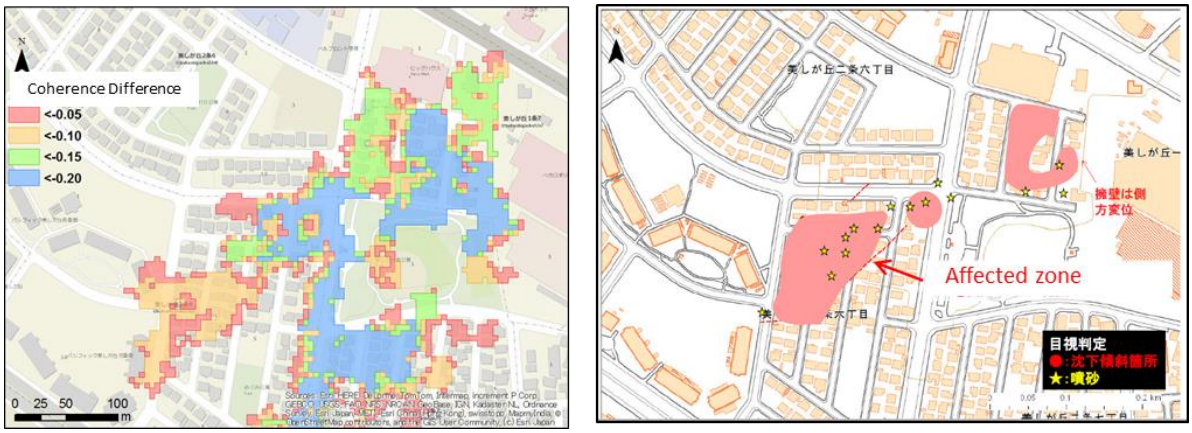

(b) Utsukushigaoka

Figure 6. Extraction of liquefaction affected areas by four thresholds of the coherence difference (left) in (a) Satozuka and (b) Utsukushigaoka and the corresponding field survey results (right) by Nishimura and Watanabe (2018)

The average value and the standard deviation of the coherence difference in Fig. 5(a) are 0.01 and 0.08, respectively. These values are very small and close to zero. Thus the threshold values of the average to extract liquefaction affected areas were tested from four cases: -0.05, -0.10, -0.15, and -0,20. To remove the effects cars in the coherence difference, the extracted areas smaller than 2,500 m^2 were removed as noises. These threshold values were examined for Satozuka and Utsukushigaoka areas in Fig. 6 together with the result of field survey by Nishimura and Watanabe (2018). Note that this survey was conducted soon after the occurrence of the earthquake, and hence it is considered to be more suitable ground truth than ours.

In Satozuka, a ground failure zone of apparent uneven settlement could be extracted by all the four threshold values. But an accumulated sand zone could not be extracted by the threshold of -0.20. On the contrary, the areas without damage reports were also extracted by the large thresholds, e.g. -0.05 and -0.10. In Utsukushigahara, wider areas were extracted from the coherence difference than the field survey result. The northern area of the park was extracted by all the thresholds but the western part was extracted only by larger thresholds, e.g. -0.05 and -0.10. Considering these comparisons, the threshold -0.15 was selected as the most suitable value of the coherence difference to extract the damages associated by ground failures in this study.

Using this threshold -0.15, affected areas were estimated for the study area in Fig. 5(b) and the result is shown in Fig. 7 together with the observed ground failure locations by Nishimura and Watanabe (2018). The extracted locations in this study agree well with the field survey data. Thus the use of three-temporal coherence values is considered to be useful to extract ground failures in urban areas.

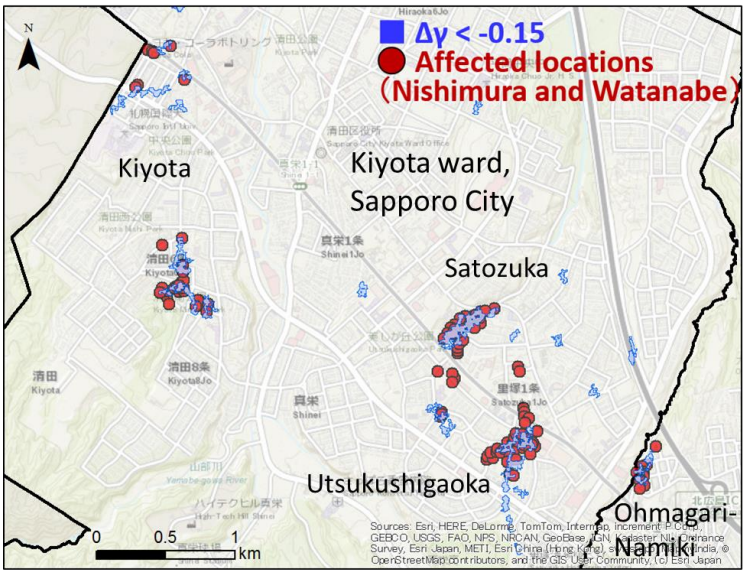

Figure 7. Comparison of the affected areas estimated by coherence difference -0.15 in this study and the field survey result by Nishimura and Watanabe (2018).

CONCLUSIONS

A JMA magnitude 6.7 earthquake hit the eastern Iburi sub-prefecture, Hokkado, Japan, on September 6, 2018. Two pre-event and one post-event PALSAR-2 images taken 19 hours after the earthquake were used to extract affected areas due to liquefaction triggered ground failures in urban areas, Sapporo and Kita-Hiroshima Cities. The coherence values for the pre-event pair and the co-event pair were calculated, and their difference was considered as the change due to the earthquake. Urban areas with decreased coherence after the earthquake were extracted as affected areas. The threshold value of the coherence difference was discussed by comparing with the field survey reports. As the result, most of the reported damaged areas could be detected successfully using the multi-temporal SAR coherence data.

ACKNOWLEDGMENTS

The ALOS-2 PALSAR-2 data are owned by the Japan Aerospace Exploration Agency (JAXA) and were provided through the ALOS-2 research program (RA6, PI No. 3243). This work was partially supported by JST CREST Grant Number JPMJCR1411, Japan, and JSPS KAKENHI Grant Numbers 17H02066, Japan.

REFERENCES

Cabinet Office of Japan (2019). "Summary of damage due to the 2018 Hokkaido Eastern Iburi Earthquake,", http://www.bousai.go.jp/updates/h30jishin_hokkaido/pdf/310128_jishin_hokkaido.pdf (Accessed May 2019)

Dell'Acqua, F. and P. Gamba (2012). "Remote sensing and earthquake damage assessment: Experiences, limits, and perspectives," *Proceedings of the IEEE*, **100**(10), 2876-2890.

Geospatial Information Authority of Japan (2018). "the 2018 Hokkaido Eastern Iburi Earthquake," http://www.gsi.go.jp/BOUSAI/H30-hokkaidoiburi-east-earthquake-index.html (Accessed May 2019)

Ishitsuka, K., T. Tsuji and T. Matsuoka (2013). "Detection and mapping of soil liquefaction in the 2011 Tohoku earthquake using SAR interferometry," *Earth Planets Space*, **64**, 1267–1276.

Japan Aerospace Exploration Agency (2018). "Calibration Result of ALOS-2/PALSAR-2 JAXA Standard Products," https://www.eorc.jaxa.jp/ALOS-2/en/calval/calval_index.htm (Accessed May 2019)

Japan Meteorological Agency (2018). "Information on the 2018 Hokkaido Eastern Iburi Earthquake," http://www.jma.go.jp/jma/menu/20180906_iburi_jishin_menu.html (Accessed May 2019)

Liu, W., F. Yamazaki, H. Gokon and S. Koshimura (2013). "Extraction of tsunami-flooded areas and damaged buildings in the 2011 Tohoku-Oki Earthquake from TerraSAR-X intensity images," *Earthquake Spectra*, **29**(S1), S183-S200.

Liu, W. and F. Yamazaki (2017). "Extraction of collapsed buildings due to the 2016 Kumamoto earthquake based on multi-temporal PALSAR-2 data," *Journal of Disaster Research*, **12**(2), 241-250.

National Research Institute for Earth Science and Disaster Resilience (2018). "Crisis response site of the 2018 Hokkaido Eastern Iburi Earthquake," http://crs.bosai.go.jp/DynamicCRS/index.html?appid=5a555e4a581c4e2885b59a658535fd3e (Accessed May 2018)

Nishimura, S. and Y. Watanabe (2018). "Liquefaction damage in the 2018 Hokkaido Eastern Iburi Earthquake," https://www.jiban.or.jp/wp-content/uploads/2018/10/nishimura_watabe_20181002.pdf (Accessed May 2018)

Rathje, E. and B.J. Adams (2008). "The role of remote sensing in earthquake science and engineering, opportunities and challenges," *Earthquake Spectra*, **24**(2), 471–492.

Tsuchida, R., W. Liu and F. Yamazaki (2015). "Detection of landslides in the 2015 Gorkha, Nepal earthquake using satellite imagery," *Proc. 36th Asian Conference on Remote Sensing*, Manila, Philippines, 10p.

Yamazaki, F. and M. Matsuoka (2007). "Remote sensing technologies in post-disaster damage assessment," *Journal of Earthquakes and Tsunamis*, **1**(3): 193-210.

Wakamatsu, K. and A. Onoue (2018). "Ground failures in Kiyota Ward, Sapporo City due to the 2018 Hokkaido Eastern Iburi Earthquake," http://home.kanto-gakuin.ac.jp/~wakamatu/wakamatsu/reports/utsukushigaoka_kiyota_report.pdf (Accessed May 2018)